HHS Public Access

Author manuscript

Water Res. Author manuscript; available in PMC 2023 February 15.

Published in final edited form as:

Water Res. 2022 February 15; 210: 117988. doi:10.1016/j.watres.2021.117988.

Pyrogenic Carbon-Promoted Haloacetic Acid Decarboxylation to Trihalomethanes in Drinking Water

Pamela Rose V. Samonte[†,1], **Zhao Li**[†,1], **Jingdong Mao**[‡], **Brian P. Chaplin**[§,▽,☆], **Wenqing Xu**[†,*]

[†]Department of Civil and Environmental Engineering, Villanova University, 800 E. Lancaster Ave., Villanova, PA 19085

[‡]Department of Chemistry and Biochemistry, Old Dominion University, Norfolk, Virginia 23529, United States

[§]Department of Chemical Engineering, University of Illinois at Chicago, 929 W. Taylor St., Chicago, IL 60607

[▽]Institute of Environmental Science and Policy, University of Illinois at Chicago, 1603 W. Taylor St., Chicago, IL 60612

[☆]Department of Civil, Materials, and Environmental Engineering, University of Illinois at Chicago, 842 W. Taylor St., Chicago, IL 60607

Abstract

Drinking water disinfection by chlorination or chloramination can result in the formation of disinfection byproducts (DBPs) such as haloacetic acids (HAAs) and trihalomethanes (THMs). Pyrogenic carbonaceous matter (PCM), such as activated carbon (AC), is commonly used as an ostensibly inert adsorbent to remove HAAs from water. HAA degradation has been mainly attributed to biological factors. This study, for the first time, revealed that abiotic HAA degradation in the presence of PCM could be important under water treatment conditions. Specifically, we observed complete destruction of Br_3AA, a model HAA, in the presence of powder AC at pH 7 within 30 min. To understand the role of PCM and the reaction mechanism, we performed a systematic study using a suite of HAAs and various PCM types. We found that PCM significantly accelerated the transformation of three HAAs (Br_3AA, $BrCl_2AA$, Br_2ClAA) at pH 7. Product characterization indicated an approximately 1:1 HAA molar transformation

[*]Corresponding author: Wenqing Xu, wenqing.xu@villanova.edu, Phone: 001-(610) 519-8549.

[1]Pamela Rose V. Samonte and Zhao Li contributed equally to this work.

Supporting Information

Text details on reagents, GC/ECD oven program, solid-phase extraction efficiencies, and HCl-washing preparation method. SI presents tables detailing Freundlich model parameters, specific surface areas, and mass fluxes; and detailed figures on adsorption kinetics, adsorption isotherms, decay kinetics, Langmuir model fitting, and pzc determination.

Declaration of Competing Interest

The authors declare that they have no known competing financial interests or personal relationships that could have appeared to influence the work reported in this paper.

into their respective THMs following a decarboxylation pathway with PCM. The Br_3AA activation energy (E_a) was measured by kinetic experiments at 15–45°C with and without a model PCM, wherein a significant decrease in E_a from 25.7±3.2 to 13.6±2.2 kcal·mol^{-1} was observed. We further demonstrated that oxygenated functional groups on PCM (*e.g.*, −COOH) can accelerate HAA decarboxylation using synthesized polymers to resemble PCM. Density functional theory simulations were performed to determine the enthalpy of activation ($\Delta H^{\ddagger}$) for Br_3AA decarboxylation with H_3O^+ and formic acid (HCOOH). The presence of HCOOH significantly lowered the overall $\Delta H^{\ddagger}$ value for Br_3AA decarboxylation, supporting the hypothesis that −COOH catalyzes the C-C bond breaking in Br_3AA. Overall, our study demonstrated the importance of a previously overlooked abiotic reaction pathway, where HAAs can be quickly converted to THMs with PCM under water treatment relevant conditions. These findings have substantial implications for DBP mitigation in water quality control, particularly for potable water reuse or pre-chlorinated water that allow direct contact between HAAs and AC during filtration as well as PAC fines traveling with finished water in water distribution systems. As such, the volatilization and relative low toxicity of volatile THMs may be considered as a detoxification process to mitigate adverse DBP effects in drinking water, thereby lowering potential health risks to consumers.

Graphical abstract

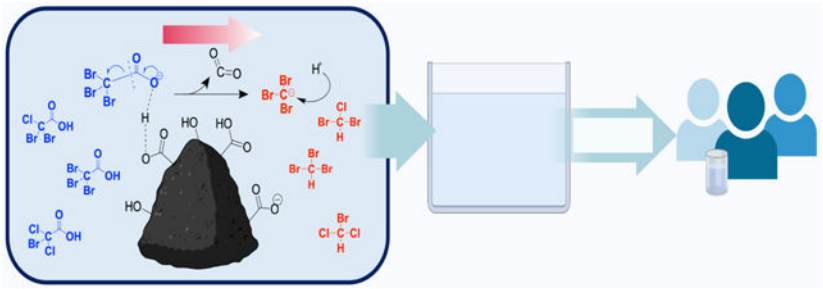

Keywords

Disinfection byproducts; haloacetic acids; trihalomethanes; decarboxylation; density functional theory; pyrogenic carbonaceous matter

1. Introduction

Haloacetic acids (HAAs) and trihalomethanes (THMs) are major classes of disinfection byproducts (DBPs) that are produced when disinfectants react with organic and inorganic precursors in water (McRae et al., 2004; Parvez et al., 2019; Zhang et al., 2015). The occurrence of HAAs and THMs have been reported in drinking water (Levesque et al., 2006; Rodriguez et al., 2004; Villanueva et al., 2003). Since the identification of the first known DBPs in the 1970s, DBPs such as HAAs and THMs have been increasingly reported to be ubiquitous in chlorinated drinking water at HAA and THM concentrations ranging between 8–86 and 3–50 μg·L^{-1}, respectively (Richardson, 2002; Villanueva et al., 2003). Due to the potential genotoxicity and carcinogenicity of HAAs (Pals et al., 2011; Parvez et al., 2019; Zhang et al., 2015), the United States Environmental Protection Agency (USEPA) currently regulates five HAAs (ClAA, Cl_2AA, Cl_3AA, BrAA, Br_2AA) and four

THMs ($CHBr_3$, $CHCl_3$, $CHBrCl_2$, $CHBr_2Cl$) in drinking water under Stages I/II of the Disinfectants/Disinfection Byproducts Rule at a combined maximum contaminant level (MCL) of 60 $\mu g \cdot L^{-1}$ for HAAs and 80 $\mu g \cdot L^{-1}$ for THMs. Four additional HAAs, namely, tribromoacetic acid (Br_3AA), bromochloroacetic acid (BrClAA), bromodichloroacetic acid ($BrCl_2AA$), and chlorodibromoacetic acid (Br_2ClAA), although not yet regulated, have raised concerns over their higher cytotoxicity and genotoxicity as compared to regulated HAAs (Plewa et al., 2010; USEPA, 2016). Thus, effective mitigative approaches toward controlling both regulated and emerging HAAs are needed.

Pyrogenic carbonaceous matter (PCM) is the solid residual generated from the incomplete combustion of fresh or fossilized biomass. Engineering analogs of PCM, such as granular activated carbon (GAC) and powder activated carbon (PAC), have been widely used in water treatment (Benjamin and Lawler, 2013). For instance, GAC/PAC (Altmann et al., 2016; Tung et al., 2006) are commonly used medium for water filtration, wherein their effectiveness largely depends on the contaminant's hydrophobicity (Golea et al., 2020; Jiang et al., 2017). Therefore, they are effective towards intermediate aromatic DBPs (Jiang et al., 2020; Jiang et al., 2018; Jiang and Zhang, 2018; Jiang et al., 2017), but are ineffective towards DBPs with high polarity and low molecular weight, such as HAAs (Tung et al., 2006) and THMs (Capar and Yetiş, 2002; Summers et al., 1993). Furthermore, once the adsorption sites are saturated, used GAC/PAC require off-site disposal or regeneration (Crittenden et al., 2012; Xie, 2003), with costs ranging from \$1,720 to \$3,000 $ton^{-1}year^{-1}$ (Casey et al., 2013; USEPA, 2000). Biological AC (BAC) is often used for HAA removal during water treatment. BAC reactivity has been attributed to biotic processes of bacterial enrichment cultures (McRae et al., 2004), heterotrophic bacteria (Hozalski et al., 2001; Tung and Xie, 2009), and biofilms (Behbahani et al., 2018; Tung and Xie, 2011; Zhou and Xie, 2002), whereas AC is considered an inert attachment surface for microbial growth. Recent studies have found that PAC incorporation into porous electrodes can mimic BAC performance by facilitating the adsorption of polar DBPs, such as HAAs and *N*-nitrosodimethylamine (NDMA), and subsequently destroying these contaminants electrochemically (Almassi et al., 2019a; Almassi et al., 2019b).

Although the role of PCM as a passive adsorbent is well-recognized, recent studies have demonstrated that PCM has intrinsic reactivity and can participate in an array of biotic and abiotic reactions occurring in the natural environment (Pignatello et al., 2017; Xu et al., 2020a; Xu et al., 2021). For instance, PCM promotes a suite of pollutant transformation under environmentally relevant conditions, including primary amines (Aguilar et al., 2005), nitroaromatics (Ding et al., 2018; Gomes et al., 2008), phenolic compounds (Li et al., 2015; Pei et al., 2018; Xie et al., 2017), chlorinated hydrocarbons (Chen et al., 2014), explosives (Xu et al., 2010), agrochemicals (Ding et al., 2019; Ding and Xu, 2016; Xu et al., 2013; Xu et al., 2022; Xu et al., 2020b), and azo dyes (van der Zee et al., 2003; Zhao et al., 2019). Given the widely observed PCM reactivity in nature, these reactions could potentially occur in engineered systems, including water treatment processes. For instance, AC was able to convert N-DBP precursors (*e.g.*, dimethylamine) to nitrosamines, increasing secondary amine formation in wastewater effluent (Padhye et al., 2010; Padhye et al., 2011). Previous studies also reported HAA conversion to their respective trihalomethanes under ambient (Heller-Grossman et al., 1993; Zhang and Minear, 2002) or high-temperature

conditions (Chen et al., 2021; Lifongo et al., 2010; Pan et al., 2014) in the absence of PCM with relatively slow kinetics, *e.g.*, a half-life of 17 d for Br_3AA (Zhang and Minear, 2002). However, despite the prevalence of BAC for HAA removal in water treatment, little information is available regarding whether or not PCM could promote abiotic HAA transformation kinetics or their associated product distribution. Characterizing and understanding how these reactions may affect HAA mitigation are important in water quality control, especially for potable water reuse or pre-chlorinated water, wherein HAAs and AC have direct contact during the filtration process, as well as clear water and well distribution systems that often present PAC fines that travel with finished water.

This study aims to investigate the feasibility of PCM in promoting abiotic HAA transformation under conditions relevant to water treatment and characterize the associated surface transformation reaction pathway. Specifically, we explored nine HAAs (HAA_9: Br_3AA, Br_2ClAA, $BrCl_2AA$, ClAA, Cl_2AA, Cl_3AA, BrAA, Br_2AA, BrClAA), including both regulated and emerging DBPs, to understand structural HAA requirements for PCM-enhanced abiotic transformation. The degradation of HAAs was monitored and their products were characterized. Kinetic modeling was performed to delineate the adsorption kinetics from surface transformation rates. The role of specific PCM functional groups (*e.g.*, −COOH, −OH) in promoting HAA transformation (*i.e.*, Br_3AA) was investigated by synthesizing PCM-like polymers to resemble PCM. Density functional theory (DFT) simulations were performed, where the enthalpy of activation ($\Delta H^{\ddagger}$) and overall reaction enthalpy (ΔH_r) for Br_3AA decarboxylation were determined. Lastly, the impact of solution chemistry was evaluated and HAA decay dependence on PCM type (*e.g.*, graphite, PAC, MWCNTs) was studied. Our findings elucidated an overlooked reaction where the presence of PCM significantly enhanced abiotic HAA transformation into their respective haloforms under water treatment relevant conditions. These results can inform the water industry regarding their DBP mitigation approaches, where the increased presence of volatile THMs with relatively lower toxicity following HAA decay might help reduce the adverse health impact of DBPs in drinking water.

2. Materials and Methods

2.1. Reagents

A complete reagent list is detailed in Text S1. PCM-like polymers were synthesized by Pd(0)/Cu(I)-catalyzed cross-coupling chemistry following a method adapted from our previous study (Li et al., 2019). Three PCM-like polymers were obtained, where PCM_0, PCM_{-OH}, and PCM_{-COOH} represent polymers with no functionality, −OH, and −COOH groups, respectively. PCM_0 was obtained by reactions where a 1,4-dibromobenzene node connected to a rigid 1,3,5-triethynylbenzene strut. Briefly, 1,3,5-triethynylbenzene (3.0 mmol), 1,4-dibromobenzene (3.0 mmol), tetrakis(triphenylphosphine)palladium(0) (150 mg), and copper(I) iodide (45 mg) were dissolved in a *N,N*-dimethylformamide (20 mL) and triethylamine (20 mL) mixture for 30 min, stored in darkness, and heated to 80°C for 72 h under nitrogen. The reactor was cooled to room temperature. The products were washed with chloroform, water, methanol, and acetone to remove unreacted monomers and catalyst residues, and purified by Soxhlet extraction with methanol for 48 h and

dried at 100°C for 24 h. PCM_{-OH} and PCM_{-COOH} were synthesized following the same route, except 2,5-dibromohydroquinone and 2,5-diiodobenzoic acid respectively substituted 1,4-dibromobenzene. PCM_0 (yield: 107%) and PCM_{-OH} (yield: 114%) were dark brown as previously reported (Li et al., 2019), and PCM_{-COOH} (yield: 86%) was light orange.

2.2. Batch adsorption experiments

A series of HAA_6 (ClAA, Cl_2AA, Cl_3AA, BrAA, Br_2AA, BrClAA) from 1–10 $mg \cdot L^{-1}$ were spiked into batch reactors (KIMAX Culture Tubes filled to 10 mL with minimal headspace) with pre-weighed PCM (30 $g \cdot L^{-1}$) in 10 mM KH_2PO_4/K_2HPO_4 (pH 7.0±0.1) to obtain a 1–2 log range isotherm curve. A model PCM, graphite, was chosen due to its high carbon purity (~99 wt%) and lack of functionality and porosity. Blank controls without graphite were simultaneously prepared. All samples were capped with Teflon-lined septa and placed on an end-to-end rugged rotator mixer (Glas-Col, Tere Haute, IN, USA) in darkness at 30 rpm, 25°C in a Model VRI6P incubator (VWR International, Radnor, PA, USA) for 24 h to allow adsorption equilibrium. The equilibrium time was determined separately by monitoring the aqueous phase HAA (*i.e.*, Br_2AA) concentration until it plateaued (Fig. S1). After 24 h, all samples were centrifuged (Forma Scientific Inc. 5678, Marietta, OH, USA) at 3,000 rpm for 3 min. HAA_6 from the aqueous phase were analyzed following the methods described in Section 2.4. Adsorption isotherms were constructed by plotting the solid phase concentration (q_e; $\mu g \cdot g^{-1}$), which was determined by a mass balance approach, versus HAA aqueous phase concentration (C_e; $\mu g \cdot L^{-1}$) at equilibrium. The isotherms were subsequently fit against the Freundlich model (Tung et al., 2006).

2.3. Batch reaction experiments

A concentration of 50 $\mu g \cdot L^{-1}$ of HAA_3 (Br_3AA, Br_2ClAA, or $BrCl_2AA$) was added to batch reactors containing pre-weighted PCM or PCM-like polymers (0.77 for PAC, MWCNTs, and PCM-like polymers; 23.08 $g \cdot L^{-1}$ for graphite) with 10 mM KH_2PO_4/K_2HPO_4 (pH 7.0±0.1) or local tap water (pH 7.0±0.2; unadjusted) for HAA_3 degradation experiments. A higher concentration of graphite was used to speed up the reaction as it has the minimum surface area and functionality of the PCM tested. For pH-dependent study, a phosphate-carbonate buffer ($KH_2PO_4/K_2HPO_4/NaHCO_3$) was used for pH 5–9, wherein $[KH_2PO_4]+[K_2HPO_4]+[NaHCO_3]$ was adjusted to 2 mM to ensure uniform ionic strength. DI water was adjusted with H_2SO_4 for pH-dependent study at pH 3. Controls without solids were simultaneously prepared. All samples were capped with Teflon-lined septa and placed on an end-to-end rugged rotator mixer in darkness (30 rpm), 25°C in an incubator. Samples were centrifuged at 3,000 rpm for 3 min at various time intervals. Both aqueous and solid phases were analyzed for HAA_3 and THM_3 ($CHBr_3$, $CHBr_2Cl$, $CHBrCl_2$) following methods described in Section 2.4.

2.4. Chemical analysis

The HAA_9 and THMs were analyzed following methods adapted from EPA method 552.3 and 551.1, respectively (USEPA, 1995; 2003). Briefly, the aqueous phase was pipetted out and adjusted to pH<0.5, and methyl tert-butyl ether (MTBE; with 200 $\mu g \cdot L^{-1}$ 1,2,3-trichloropropane (1,2,3-TCP) as internal standard) was added at a 1:1 volumetric ratio. Subsequently, HAA_9 solid-phase extraction (SPE) proceeded by adding 5 mL MTBE to

the remaining solids and 5 min vortexing. The extracted HAAs in MTBE were converted to methyl esters by adding acidic methanol (10 vol%, 18 M H_2SO_4) at a 1:1 volumetric ratio followed by 30 s vortexing and 50°C heating for 2 h. A Na_2SO_4 solution was added to remove the acidic aqueous phase and a saturated $NaHCO_3$ solution was used for solution neutralization. Fifty $\mu g \cdot L^{-1}$ 2,3-dibromopropanoic acid was added as the surrogate standard. Conversely, THM_3 liquid-liquid microextraction proceeded by adding 2 mL MTBE (containing 200 $\mu g \cdot L^{-1}$ 1,2,3-TCP) to 2-mL water samples and 2 min vortexing. THM_3 SPE proceeded by adding 5 mL MTBE, 5 min vortexing, and 3,000 rpm centrifuging for 3 min. All extracts were analyzed by gas chromatography/electron capture detection (GC/ECD) with an Rxi-5ms column (30 m×0.25 mm, 0.25 μm; Restek Inc., Bellefonte, PA, USA) and N_2 as carrier gas. GC oven program details are in Text S2. The extraction efficiencies and phase distributions for HAAs and THM_3 are in Text S3. For product identification purposes, select samples with high Br_3AA concentration (10 $mg \cdot L^{-1}$) were analyzed for bromide using ion chromatography (IC; Shimadzu, Kyoto, Japan).

2.5. Characterization of PCM and PCM-like polymers

The graphite, PAC, MWCNTs, PCM_0, PCM_{-OH}, and PCM_{-COOH} surface areas were measured following a previously established method using a Brunauer-Emmett-Teller (BET) surface analyzer NOVA 3000e (Quantachrome Instruments, Boynton Beach, FL, U.S.A.) with nitrogen at 77.3 K (Li et al., 2019) (Table S1); Particle Technology Labs (Downers Grove, IL, U.S.A.) conducted PCM_{-COOH} analysis on a Tristar II BET surface analyzer (Micrometrics, Norcross, GA, U.S.A). All samples were outgassed at 110°C for 18 h before measurement. Surface areas calculations used data collected from 0.015–0.05 p/p_0. All nuclear magnetic resonance (NMR) experiments were performed on a Bruker Avance 400 spectrometer at 100 MHz ^{13}C frequency with a double-resonance probe head with 4-mm sample rotors. A previously established ^{13}C multiple cross-polarization/magic angle spinning (multi-CP/MAS) NMR technique was applied to gather PCM-like polymer quantitative structural information (Johnson and Schmidt-Rohr, 2014; Li et al., 2019), wherein analysis was performed to investigate the polymerization degree (Mao and Schmidt-Rohr, 2003; Tang et al., 2000). The quantitative spectra were recorded at a spinning speed of 14 kHz and 90° ^{13}C pulse length of 4 μs. All spectra presented good signal-to-noise ratios with significantly small (<3%) spinning sidebands and minimal overlapping center bands. In addition, the multi-CP experiments were combined with 68 μs dipolar dephasing (multi-CP/DD) to generate non-protonated C and mobile group sub-spectra (Johnson and Schmidt-Rohr, 2014; Li et al., 2019).

We adapted a previously established method to determine the point-of-zero charges (pzc) for PCM and PCM-like polymers (Ni et al., 2011). Briefly, DI water, wherein all reagents and NaOH and HCl solutions were prepared, was boiled for 1 h and degassed with N_2 for 30 min for CO_2 removal. Subsequently, 0.8 g powder (graphite, PCM_{-OH}, or PCM_{-COOH}) was pre-wetted in 10 mL DI water for 48 h at 25°C, 40 rpm. The initial blank pH (no solids) with 10 mL DI water was lowered to pH~2, and recorded volumes of 0.1 or 1 N NaOH were added until pH~12. Identical HCl and NaOH volumes were added to each powder sample, and the pH at each increment was recorded. The powder pzc was obtained when the initial and final pH values were identical.

2.6. Density functional theory (DFT) simulations

Density functional theory (DFT) simulations were performed using Gaussian 16 software (Frisch, 2016). Unrestricted spin, all-electron calculations were performed using the 6–31G+(d) basis set for frequency and geometry optimizations, and the 6–311G+(3df, 2p) basis set for energy calculations. M06-2X hybrid meta exchange-correlation functionals were employed for exchange and correlation. This combination of basis sets and correlation functionals has been shown to be accurate for estimating reactions of organic compounds (Foresman and Frisch, 1996; Zhao and Truhlar, 2008). Implicit water solvation was simulated using the solvation model based on solute electron density (SMD) (Marenich et al., 2009). The transition state of a given reaction was determined by the pseudo-reaction coordinate method (Anderson and Kang, 1998), where the C-C bond length in $Br_3C\text{-}COO^-$ was systemically varied. The resulting structure was confirmed to be representative of the transition state by yielding a single negative frequency during the frequency calculation (Foresman and Frisch, 1996).

3. Results and Discussion

3.1. Br_3AA, Br_2ClAA, and $BrCl_2AA$ transformation kinetics and products

Three out of nine HAAs (HAA_3: Br_3AA, Br_2ClAA, $BrCl_2AA$) exhibited reactivity toward graphite. By contrast, degradation was not observed for the other six HAAs (HAA_6). Consistent with a previous study (Almassi et al., 2019b), HAA_6 adsorption can be described by the Freundlich model (adsorption isotherms in Fig. S2). HAA_3 decay was monitored over time to obtain over 90% parent compound decay. The total Br_3AA mass from both solid and aqueous phases were obtained using previously determined extraction efficiencies (Text S3). Our results suggest that the presence of graphite significantly accelerated Br_3AA decay, where (80.5±0.01)% of Br_3AA disappeared with graphite compared to (38.7±0.01)% without graphite over the experimental timeframe (Fig. 1a,1b). HAA degradation without graphite has been previously reported to follow an intramolecular electron transfer reaction (Zhang and Minear, 2002). Bromoform ($CHBr_3$) was identified as the main Br_3AA transformation product, with a 1:1 molar transformation of Br_3AA to $CHBr_3$. The average mass balance on bromine atom, calculated as $3[Br_3AA]+3[CHBr_3]$, was close to 100% over the entire experimental timeframe with/without graphite.

Similarly to Br_3AA, graphite also accelerated Br_2ClAA and $BrCl_2AA$ decay but with much slower kinetics. Details on HAA_3 pseudo first-order decay kinetics and R^2 values are in Fig. S3. Similar to Br_3AA, a 1:1 molar transformation of Br_2ClAA and $BrCl_2AA$ to their respective THMs, $CHBr_2Cl$ and $CHBrCl_2$, were observed. Approximately 100% Br mass balance, calculated as $2[Br_2ClAA]+2[CHBr_2Cl]$ and $[BrCl_2AA]+[CHBrCl_2]$, were achieved for Br_2ClAA and $BrCl_2AA$, respectively. To characterize the formation of other transformation products, select samples with high Br_3AA concentration (10 $mg{\cdot}L^{-1}$) were monitored with or without graphite, wherein no Br^-, Br_2AA, BrAA, or acetic acid were observed, suggesting reductive dehalogenation was negligible (Adhikary et al., 2017; Hozalski et al., 2001) for all reaction systems with/without graphite.

As shown in Fig. 1c, k_{obs} for HAA_3 decay with graphite followed the trend: Br_3AA ($(2.02\pm0.17)\times10^{-1}$ d^{-1}; R^2=0.97) > Br_2ClAA ($(4.75\pm0.88)\times10^{-2}$ d^{-1}; R^2=0.85) > $BrCl_2AA$ ($(1.03\pm0.15)\times10^{-2}$ d^{-1}; R^2=0.92). HAA_3 decay without graphite exhibited a similar trend with much slower kinetics: Br_3AA ($(4.62\pm0.64)\times10^{-2}$ d^{-1}; R^2=0.91) > Br_2ClAA ($(1.77\pm0.43)\times10^{-2}$ d^{-1}; R^2=0.86) > $BrCl_2AA$ ($(3.88\pm0.58)\times10^{-3}$ d^{-1}; R^2=0.90). HAA_3 enhancement factors by graphite were calculated by a ratio of the observed rate constants (k_{obs}) with/without graphite (*i.e.*, $k$graphite/k_{no} graphite), which followed: Br_3AA (4.37±0.25) > Br_2ClAA (2.68±0.16) > $BrCl_2AA$ (2.65±0.01).

Although haloform formation from HAA decay without PCM has been previously reported (Heller-Grossman et al., 1993; Lifongo et al., 2010; Zhang and Minear, 2002), this is the first study to demonstrate that PCM can significantly enhance the decay kinetics of these reactions. For instance, graphite shortened Br_3AA half-lives from 15±1.1 to 3.4±0.4 d. Notably, graphite was used herein as a model PCM with the smallest surface area (orders of magnitude lower than PAC) and minimum surface functionality. It is expected that HAA decay would be much faster in the presence of PAC, which will be further evaluated in Section 3.4. Moreover, the observed HAA_3 degradation trend mirrored their logK_{ow} values (Br_3AA (1.71) > Br_2ClAA (1.62) > $BrCl_2AA$ (1.53)), suggesting that non-specific interaction between HAAs and the PCM surface played a dominant role in accelerating their decay. We also investigated the possible contribution of trace metals on graphite to HAA decay, wherein no significant differences were observed in Br_3AA decay rates (k_{obs}) with graphite as a reference ($(2.68\pm0.21)\times10^{-1}$ d^{-1}; R^2=0.97)) versus HCl-washed graphite ($(2.89\pm0.29)\times10^{-1}$ d^{-1}; R^2=0.95)). Details on the experimental procedure and decay kinetics with HCl-washed graphite are in Fig. S4.

3.2. Modeling HAA decomposition on PCM surface

In general, HAA transformation with PCM is a combination of three processes (*i.e.*, adsorption, desorption, and surface transformation reactions on PCM), which can be described by the Langmuir kinetic model (Ding et al., 2018; Li et al., 2019; Xu et al., 2013):

$$\frac{dq}{dt} = k_a C(Q - q) - k_d - k_{rxn} q \qquad \text{Equation (1)}$$

where q is the HAA solid phase concentration (μg·g^{-1}), C is the aqueous concentration (μg·L^{-1}), Q is the total number of sorption sites (μg·g^{-1}), and k_a (L·μg^{-1}·d^{-1}), k_d (d^{-1}), and k_{rxn} (d^{-1}) are the adsorption, desorption, and surface transformation reaction rate constants, respectively. Depending on the rate-limiting step among these processes, k_{obs} may not reflect the true surface transformation reaction rate (k_{rxn}). Thus, we used a combined modeling and experimental approach to quantify k_{rxn}. Br_3AA was employed as a model compound herein. Details on the model fitting are in Text S4, Fig. S5 and obtained rate constants for Br_3AA adsorption, desorption, and surface transformation reaction with graphite are in Table 1.

Our results suggest a three-fold larger k_{rxn} ($(3.52\pm0.92)\times10^{2}$ d^{-1}) as compared to k_{obs} ($(2.02\pm0.17)\times10^{-1}$ d^{-1}) for Br_3AA decay with graphite, suggesting that the adsorption

process is rate-limiting (Table 1). Moreover, we calculated the Br_3AA mass fluxes (ϕ; $\mu g \cdot m^{-2} \cdot d^{-1}$) for the surface transformation reaction ($\phi_{rxn}=k_{rxn}q$), adsorption ($\phi_a=k_aC(Q-q)$), and desorption ($\phi_d=k_dq$) with graphite (Table S2). Across the experimental timeframe, all mass flux terms were comparable with each other, suggesting that all three processes contributed to Br_3AA transformation and thus the observed k_{obs} with graphite.

3.3. Reaction mechanism

3.3.1. Activation energy (E_a)—A previous study suggested that HAA conversion to THMs followed intramolecular electron transfer (Zhang and Minear, 2002). In our study, the presence of PCM evidently accelerated the reaction. To understand the role of PCM in accelerating Br_3AA degradation, we first quantified the activation energy (E_a) of Br_3AA decarboxylation by measuring Br_3AA decay rate constants over 15–45°C with and without graphite. Detailed decay kinetics are in Fig. S6. Eq. 2 can be linearized to calculate E_a:

$$k_{obs} = Ae^{-\frac{E_a}{RT}} \quad \text{Equation (2)}$$

where k_{obs} is the degradation rate constant (d^{-1}), A is the pre-exponential factor (d^{-1}), E_a is the activation energy ($kcal \cdot mol^{-1}$), R is the gas constant, and T is the temperature (K).

As shown in Fig. 2a, graphite accelerated Br_3AA decay from 15 to 45°C as compared to without graphite, though the PCM effect was less predominant at higher temperatures. We determined the Br_3AA decay E_a values using the linear regression slopes, which were 13.6±2.2 and 25.7±3.2 $kcal \cdot mol^{-1}$ with and without graphite, respectively. Our results suggest that graphite significantly lowered E_a and thus accelerated Br_3AA decay. The obtained E_a without graphite was comparable to a previous study, which reported an E_a of 29.2 $kcal \cdot mol^{-1}$ for Br_3AA decarboxylation in water (Zhang and Minear, 2002). This is the first study showing that graphite could lower Br_3AA activation energy.

3.3.2. Br_3AA decay with functionalized PCM-like polymers—In this study, we employed PCM-like polymers to understand the role of oxygenated functional groups in accelerating HAA decay. By doing so, we were able to isolate specific functionalities from an array of functional groups typically present in PCM. Like PCM, the PCM-like polymers are (1) highly conjugated and amorphous with no long-range molecular order, (2) contain micropores and large surface areas, and (3) have a high affinity towards organic contaminants. Different from PCM, however, specific functional groups can be introduced via a polymer synthesis approach following protocols established in our lab (Li et al., 2019), allowing us to investigate the impact of individual functionalities on HAA decay.

Advanced solid-state ^{13}C NMR spectroscopy was used to provide information on the polymerization degree and confirm the presence of target functional groups. As shown in Fig. 2b, peaks at 123.7 ppm (C_{Ar}–C C–C_{Ar}), 131.8 ppm (C_{Ar-H}), and 90.8 ppm ($C_{R\text{-}C\equiv C\text{-}R'}$) suggest conjugated polymer network formation in PCM, $PCM_{\text{-}OH}$, and $PCM_{\text{-}COOH}$. Additionally, peaks at 167.8 ppm (C_{Ar-OH}) and 196.2 ppm ($C_{Ar=O}$) for $PCM_{\text{-}OH}$ respectively verify the incorporation of phenolic and carbonyl groups in the polymer network. Peak-differentiation-imitating NMR analysis was employed to investigate

the polymerization degree (Li et al., 2019). Specifically, the peak at 90.8 ppm ($C_{R\text{-}C\equiv C\text{-}R'}$) indicates efficient aryl halide and alkyne coupling. The low-intensity peak ratio at 80.3 ppm ($C_{-C\equiv C-H}$) over the peak at 90.8 ppm ($C_{R\text{-}C\equiv C\text{-}R'}$) provides information on the condensation degree, wherein smaller values indicate higher polymerization degrees. PCM_0 and $PCM_{\text{-}OH}$ exhibited ratios of 0.18 and 0.15, respectively, as previously reported (Li et al., 2019), and $PCM_{\text{-}COOH}$ presented a ratio of 0.01, suggesting a higher condensation degree, which were consistent with previous literature (Dawson et al., 2009; Jiang et al., 2008).

To understand the influence of oxygenated functional groups on HAA sorption and decay, the Br_3AA reactivity against PCM_0, $PCM_{\text{-}OH}$, and $PCM_{\text{-}COOH}$ was examined. Br_3AA demonstrated pseudo first-order decay at pH 7 with PCM-like polymers (Fig. 2c): $PCM_{\text{-}COOH}$ (k_{obs}=(4.31±0.05)×10^{-1} d^{-1}; R^2=0.92) > $PCM_{\text{-}OH}$ ((3.58±0.62)×10^{-1} d^{-1}; R^2=0.84) > PCM_0 ((2.57±0.20)×10^{-1} d^{-1}; R^2=0.98). The kinetics of Br_3AA decay, product formation, and bromine mass balance in the presence of PCM_0, $PCM_{\text{-}OH}$, and $PCM_{\text{-}COOH}$ are shown in Fig. S7, where ~100% Br mass balance were observed with all PCM-like polymers. Given that all polymers were synthesized following the same reaction route with an identical catalyst, we attribute the observed differences to variations in polymer surface functionalities. Similarly to Section 3.2, we obtained the Br_3AA adsorption (k_a), desorption (k_d), and surface transformation reaction (k_{rxn}) rate constants with PCM_0, $PCM_{\text{-}OH}$, and $PCM_{\text{-}COOH}$ (Table 1). Details on Br_3AA adsorption kinetics with PCM_0, $PCM_{\text{-}OH}$, and $PCM_{\text{-}COOH}$ are in Fig. S8. Br_3AA adsorption kinetics followed: PCM_0 (k_a=(1.60±0.32)×10^{-1} d^{-1}) > PCM-$_{OH}$ ((9.29±0.68)×10^{-2} d^{-1}) > $PCM_{\text{-}COOH}$ ((6.58±0.13)×10^{-2} d^{-1}), which can be attributed to a combination of hydrophobic and electrostatic interactions between Br_3AA and PCM-like polymers. The measured pzc of $PCM_{\text{-}COOH}$ and $PCM_{\text{-}OH}$ were 2.57 and 7, respectively (Fig. S9). Thus, $PCM_{\text{-}COOH}$ is more negatively-charged compared to $PCM_{\text{-}OH}$ under circumneutral conditions, repelling negatively-charged Br_3AA (pK_a=0.72) and hindering its adsorption (Serjeant and Dempsey, 1979). Interestingly, despite the slowest adsorption rate constant for $PCM_{\text{-}COOH}$, its k_{rxn} was the highest: $PCM_{\text{-}COOH}$ (k_{rxn}=(4.34±0.01)×10^3 d^{-1}) > $PCM_{\text{-}OH}$ ((1.97±0.03)×10^3 d^{-1}) > PCM_0 ((2.68±0.01)×10^2 d^{-1}). We also calculated the mass fluxes (ϕ; μg·(m^2·d)$^{-1}$) of Br_3AA adsorption, desorption, and surface transformation reactions (Table S3). For PCM_0, ϕ_a was approximately twice compared to ϕ_{rxn}. Interestingly, ϕ_{rxn} became predominant for $PCM_{\text{-}OH}$ (ϕ_a<ϕ_{rxn}) and $PCM_{\text{-}COOH}$ (ϕ_a<<ϕ_{rxn}). These results further confirmed that adsorption was the rate-limiting step for Br_3AA decay with $PCM_{\text{-}OH}$ and $PCM_{\text{-}COOH}$ and the surface transformation rate was much higher than the k_{obs}.

3.3.3. DFT modelling—To understand the reaction pathway for Br_3AA decarboxylation, DFT simulations were performed. The enthalpy of activation ($\Delta H^{\ddagger}$) and overall reaction enthalpy (ΔH_r) were determined for Br_3AA reaction with H_3O^+ according to Reaction (1):

$$Br_3C\text{-}COO^- + H_3O^+ \rightarrow Br_3CH + CO_2 + H_2O \qquad \text{Reaction (1)}$$

where $\Delta H^{\ddagger}$=50 kcal·mol^{-1} and ΔH_r=−3.8 kcal·mol^{-1}. The C-C bond in Br_3AA increased from 1.55 to 2.00 Å in the transition state structure, wherein H^+ transfer from H_3O^+ to $-CBr_3$ was characterized (Fig. 2d-i). To investigate the ability of −COOH in catalyzing the reaction, the DFT simulations added formic acid per Reaction (2):

$$Br_3C\text{-}COO^- + HCOOH \rightarrow Br_3CH + CO_2 + HCOO^- \quad \text{Reaction (2)}$$

where $\Delta H^{\neq}$=27 kcal·mol^{-1} and ΔH_r=3.4 kcal·mol^{-1}. The Br_3AA C-C bond increased from 1.58 to 2.32 Å in the transition state structure, wherein H^+ transfer from HCOOH to $-CBr_3$ was also observed (Fig. 2d-ii). The lower $\Delta H^{\neq}$ value for Reaction (2) relative to Reaction (1) supports our experimental observation where the E_a value for Br_3AA decreased from 25.7±3.2 to 13.6±2.2 kcal·mol^{-1} with graphite. Moreover, our DFT simulation supports that −COOH catalyzes the C-C bond-breaking reaction of Br_3AA while facilitating the transfer of H^+ from −COOH to $-CBr_3$.

We postulate that the formation of a low barrier H-bond (LBHB) between Br_3AA and the surface oxygenated functional groups, −COOH in particular, played an important role in catalyzing C-C bond breaking. The LBHB strength is highly dependent on the proton affinity (pK_a) proximities of the proton donor and acceptor groups, where smaller differences in acidity constants generate stronger H-bonds (Brück et al., 2000; Pignatello et al., 2017). Thus, the higher HAA reactivity with $PCM_{\text{-}COOH}$ versus $PCM_{\text{-}OH}$ can be explained by the formation of a stronger H-bond between Br_3AA and ⧚~COOH as evidenced by the closer proximity of pK_a values between Br_3AA (0.72) and ⧚~COOH ($pK_{a,COOH}$=3–6) compared to ⧚~OH ($pK_{a,phenol}$=9–10) (Pignatello et al., 2017). In addition to surface functionalities, other reaction sites such as surface edges may also contribute to accelerating HAA decay (Luo and Jean-Charles, 2006; Pignatello et al., 2017).

3.4. PCM Type

Other PCM types, including PAC and MWCNTs, were also investigated with respect to their ability to promote Br_3AA transformation at pH 7.0, wherein k_{obs} was normalized with respect to PCM dosage (Fig. 3a; **left axis**) vs. surface area (Fig. 3a; **right axis**). Details on the 1:1 molar transformation of Br_3AA to $CHBr_3$ with PAC and MWCNTs are in Fig. S10. Our results suggest that Br_3AA decay on a dosage-normalized rate constant basis was over two orders of magnitude higher with PAC than that with MWCNTs, which was one order and three orders magnitude higher than that with the PCM-like polymers and graphite, respectively. Normalizing these rate constants once more with respect to surface area, we now see the values showed overall smaller variations among different PCM: PAC was now one order of magnitude higher than MWCNTs, which was about one order of magnitude higher than functionalized PCM-like polymers and two orders of magnitude higher than graphite. We attributed the lowest reactivity of graphite to its smallest surface area and functional groups among all PCM. These results suggest that in addition to PCM surface area, other PCM properties such as the identity and density of surface functional groups as well as surface defects (Luo and Jean-Charles, 2006; Pignatello et al., 2017) might also contribute to the PCM-accelerated HAA decay. Detailed rate constants normalized against PCM dosage and surface area are presented in Table S4.

It is possible that there might be radicals present on the PCM surface, which could initiate the formation of a carboxylate radical and thus lead to the subsequent decarboxylation of Br_3AA. We thereby performed quenching experiments by monitoring Br_3AA degradation in the presence of PAC with and without 2-propanol-d_8, as detailed in Fig. S11 and

Text S5. A statistical analysis (t-test) indicated no significant differences between the two rate constants of HAA decay ($p>0.05$) with ($(3.26\pm0.19)\times10^{-1}$ min^{-1}) or without 2-propanol-d_8 ($(3.66\pm0.25)\times10^{-1}$ min^{-1}). Moreover, the statistical analysis (t-test) indicated no significant differences ($p>0.05$) in $CHBr_3$ formation with ($6.75\pm0.93)\times10^{-4}$ μmol) or without ($7.70\pm0.38)\times10^{-4}$ μmol) 2-propanol-d_8 following a 3-min reaction of Br_3AA in the presence of PAC in a separate experiment. Our results clearly demonstrate that the radical pathway, if present, is negligible for the observed conversion between HAAs to THMs.

3.5. Effect of solution chemistry on Br_3AA degradation

We further investigated the effect of solution chemistry on Br_3AA decay kinetics under a pH range of 3–9. All pH values were measured before and after reaction, which exhibited negligible change. We observed pseudo first-order Br_3AA decay with graphite from pH 5 to 9, wherein k_{obs} followed: pH 5.2 (k_{obs} =$(2.46\pm0.25)\times10^{-1}$ d^{-1}; R^2=0.96) ≈ 6.2 (2.30 ± 0.01) $\times10^{-1}$ d^{-1}; R^2=0.99) ≈ 7.3 ($2.22\pm0.18)\times10^{-1}$ d^{-1}; R^2=0.97) ≈ 8.9 ($1.97\pm0.18)\times10^{-1}$ d^{-1}; R^2=0.96) (Fig. 3b). A statistical analysis (t-test) indicated no significant differences among the four rate constants ($p>0.05$), suggesting negligible pH effect on Br_3AA decay with graphite at pH 5–9. By contrast, a much higher k_{obs} was noted ($k_{obs,pH3}$=1.49 ± 0.16 d^{-1}; R^2=0.92) for Br_3AA degradation with graphite at pH 3. Details on Br_3AA decay kinetics with/without graphite from pH 3–9 are in Fig. S12. A previous study found negligible solution pH effect for Br_3AA degradation between pH 6–9 in water (k_{obs}=0.04–0.043 d^{-1}) (Zhang and Minear, 2002). Our results confirmed that similar trend held true for Br_3AA decay from pH 5–9 with graphite but not when the pH was lowered to 3. We attributed the accelerated Br_3AA decay observed at pH 3 to the interaction between graphite and Br_3AA. Since the pzc charge of graphite was 3.5 (Fig. S9), graphite will be negatively-charged at pH 5–9, repelling HAA and resulting in slow adsorption in the respective pH range. However, graphite will be neutral/positively-charged at pH 3, resulting in higher affinity toward HAA due to electrostatic interaction and accelerating HAA decay (Punyapalakul et al., 2009).

We also examined the water matrix effect on Br_3AA decay using local tap water (pH 7.0 ± 0.2; unadjusted). Br_3AA removal with graphite in tap water exhibited pseudo first-order kinetics (k_{obs}=0.291 ± 0.01 d^{-1}; R^2=0.99). The obtained value is comparable to the reference value in KH_2PO_4/K_2HPO_4 buffer at pH 7 (k_{obs}=0.226 ± 0.02 d^{-1}; R^2=0.97), suggesting negligible water matrix effects on Br_3AA decay with graphite. Details on Br_3AA decay kinetics with tap water and relevant parameters are in Fig. 3c. Similarly, the presence of Suwannee River natural organic matter (NOM; 3 $mg{\cdot}L^{-1}$ as C; pre-equilibrated with graphite overnight) did not affect Br_3AA decay, as evidenced by the decay kinetics in Fig. 3d. Consistent with previous studies, our results suggest negligible water matrix effects on HAA decay with NOM (Zhang and Minear, 2002).

4. Conclusions

The present study, for the first time, demonstrated that PCM alone can significantly accelerate abiotic HAA decarboxylation reaction. Although HAA decarboxylation in water alone has been previously reported, the half-lives were too slow to affect engineering applications (*e.g.*, a half-life of 15 ± 1.1 d for Br_3AA in water at pH 7). Herein, we

demonstrated that complete Br_3AA degradation removal can be achieved within the typical empty bed contact time (EBCT) of the filtration process (*i.e.*, 30 min or less) in the presence of PAC, which suggests that the AC can significantly influence the conversion of HAAs to their respective THMs in potable water reuse or pre-chlorinated water during the filtration process where HAAs are in direct contact with AC. Moreover, PAC fines may travel with the finished water in clear well and water distribution systems with a typical residence time of hours to days (Tinker et al., 2009), increasing the contact time between HAAs and PAC and further promoting the transformation of HAAs to their respective THMs. We expect these reactions to proceed even faster in residential hot water distribution systems, resulting in increased presence of volatile DBPs in treated water following HAA decay. In addition, GAC filters are widely used as home filters, where HAAs might be further converted to THMs in the time frame of minutes to hours (WQA, 2016). It has been recently reported that volatile DBPs contributed marginally to the developmental toxicity of DBP mixtures in drinking water (Han and Zhang, 2018; Li et al., 2020; Plewa and Wagner, 2015; Wagner and Plewa, 2017). Therefore, both the volatilization and the relative low toxicity of volatile THMs might contribute as a detoxification process for mitigating the adverse effects of DBPs in drinking water and thus reduce health risks to consumers.

We also employed a combined experimental and computational approach to elucidate the role of PCM in accelerating Br_3AA decarboxylation. Specifically, this study is the first to demonstrate that the presence of PCM lowered the activation energy for Br_3AA decarboxylation. We further demonstrated that the carboxylic acid groups on PCM catalyzed Br_3AA decarboxylation using a polymer synthesis approach. Our DFT simulation supported these experimental observations and showed a lower overall $\Delta H^{\ddagger}$ value for catalyzed Br_3AA decarboxylation with HCOOH versus with H_3O^+, indicating that −COOH catalyzed the C-C bond breaking of Br_3AA while facilitating H^+ transfer from −COOH to $-CBr_3$.

Overall, this study unraveled a previously overlooked process, namely the abiotic HAA conversion to their respective THMs in the presence of PCM, which could significantly affect the DBP mitigative approaches due to the rapid conversation of hydrophilic DBPs into their respective volatile DBPs. Its implications on smaller-scale applications such as home heaters or in-home granular AC filters require future investigation.

Supplementary Material

Refer to Web version on PubMed Central for supplementary material.

Acknowledgements

W.X. acknowledges the U.S. National Science Foundation CAREER award (CBET-1752220) and the National Institute of Health award (1R01ES032671-01) for financial support. W.X. and B.P.C. would also like to thank the Water Innovation Network for Sustainable Small Systems (WINSSS) for the provided funds. P.R.V.S., Z.L., and W.X. acknowledge Prof. John Sivey at Towson University for his inputs on the method analysis and reaction mechanism and Prof. Charles Coe at Villanova University for his help with the BET surface measurements. The graphical abstract was created with BioRender.com.

REFERENCES

Adhikary J, Meistelman M, Burg A, Shamir D, Meyerstein D and Albo Y 2017. Reductive dehalogenation of monobromo- and tribromoacetic acid by sodium borohydride catalyzed by gold nanoparticles entrapped in sol–gel matrices follows different pathways. European Journal of Inorganic Chemistry 2017(11), 1510–1515.

Aguilar C, García R, Soto-Garrido G and Arraigada R 2005. Catalytic oxidation of aqueous methyl and dimethylamines by activated carbon. Topics in Catalysis 33(1–4), 201–206.

Almassi S, Li Z, Xu W, Pu C, Zeng T and Chaplin BP 2019a. Simultaneous adsorption and electrochemical reduction of N-nitrosodimethylamine using carbon-Ti4O7 composite reactive electrochemical membranes. Environmental Science & Technology 53(2), 928–937. [PubMed: 30547581]

Almassi S, Samonte PRV, Li Z, Xu W and Chaplin BP 2019b. Mechanistic investigation of haloacetic acid reduction using carbon-Ti4O7 composite reactive electrochemical membranes. Environ Sci Technol.

Altmann J, Rehfeld D, Trader K, Sperlich A and Jekel M 2016. Combination of granular activated carbon adsorption and deep-bed filtration as a single advanced wastewater treatment step for organic micropollutant and phosphorus removal. Water Res 92, 131–139. [PubMed: 26849316]

Anderson AB and Kang DB 1998. Quantum Chemical Approach to Redox Reactions Including Potential Dependence: Application to a Model for Hydrogen Evolution from Diamond. The Journal of Physical Chemistry A 102(29), 5993–5996.

Behbahani M, Lin B, Phares TL and Seo Y 2018. Understanding the impact of water distribution system conditions on the biodegradation of haloacetic acids and expression of bacterial dehalogenase genes. (1873–3336 (Electronic)).

Benjamin MM and Lawler DF (2013) Water Quality Engineering : Physical / Chemical Treatment Processes, John Wiley & Sons, Incorporated, New York, UNITED STATES.

Brück A, McCoy LL and Kilway KV 2000. Hydrogen bonds in carboxylic acid–carboxylate systems in solution. 1. In anhydrous, aprotic media. Organic Letters 2(14), 2007–2009. [PubMed: 10891216]

Capar G and Yetiş U 2002. Removal of THM precursors by GAC: Ankara case study. Water Res 36(5), 1379–1384. [PubMed: 11902794]

Casey B, Bishop M, Rosenfeldt E and Reinert A 2013 Comparing carbon options for DBP control, One Water Ohio, One Water Ohio.

Chen B, Jiang J, Yang X, Zhang X and Westerhoff P 2021. Roles and knowledge gaps of point-of-use technologies for mitigating health risks from disinfection byproducts in tap water: A critical review. Water Research 200, 117265. [PubMed: 34091221]

Chen W, Zhu D, Zheng S and Chen W 2014. Catalytic effects of functionalized carbon nanotubes on dehydrochlorination of 1,1,2,2-tetrachloroethane. Environ Sci Technol 48(7), 3856–3863. [PubMed: 24617768]

Crittenden JC, Rhodes Trussell R, Hand DW, Howe KJ and Tchonobanoglous G (2012) MWH's water treatment principles and design, John Wiley & Sons, Hoboken, N.J.

Dawson R, Laybourn A, Clowes R, Khimyak YZ, Adams DJ and Cooper AI 2009. Functionalized conjugated microporous polymers. Macromolecules 42(22), 8809–8816.

Ding K, Byrnes C, Bridge J, Grannas A and Xu W 2018. Surface-promoted hydrolysis of 2,4,6-trinitrotoluene and 2,4-dinitroanisole on pyrogenic carbonaceous matter. Chemosphere 197, 603–610. [PubMed: 29407823]

Ding K, Duran M and Xu W 2019. The synergistic interaction between sulfate-reducing bacteria and pyrogenic carbonaceous matter in DDT decay. Chemosphere 233, 252–260. [PubMed: 31176126]

Ding K and Xu W 2016. Black Carbon Facilitated Dechlorination of DDT and its Metabolites by Sulfide. Environ Sci Technol 50(23), 12976–12983. [PubMed: 27934256]

Foresman JB and Frisch E (1996) Exploring Chemisitry with Electronic Structure Methods, Gaussiian Inc., Pittsburgh, PA.

Frisch MJT, G. W.;Schlegel HB; Scuseria GE; Robb MA; Cheeseman JR; Scalmani G; Barone V; Petersson GA; Nakatsuji H; Li X; Caricato M; Marenich AV; Bloino J; Janesko BG; Gomperts R; Mennucci B; Hratchian HP; Ortiz JV; Izmaylov AF; Sonnenberg JL; Williams-Young D; Ding

F; Lipparini F; Egidi F; Goings J; Peng B; Petrone A; Henderson T; Ranasinghe D; Zakrzewski VG; Gao J; Rega N; Zheng G; Liang W; Hada M; Ehara M; Toyota K; Fukuda R; Hasegawa J; Ishida M; Nakajima T; Honda Y; Kitao O; Nakai H; Vreven T; Throssell K; Montgomery JA Jr.; Peralta JE; Ogliaro F; Bearpark MJ; Heyd JJ; Brothers EN; Kudin KN; Staroverov VN; Keith TA; Kobayashi R; Normand J; Raghavachari K; Rendell AP; Burant JC; Iyengar SS; Tomasi J; Cossi M; Millam JM; Klene M; Adamo C; Cammi R; Ochterski JW; Martin RL; Morokuma K; Farkas O; Foresman JB; Fox DJ 2016. Gaussian 16, Revision B.01, Gaussian, Inc., Wallingford CT.

Golea DM, Jarvis P, Jefferson B, Moore G, Sutherland S, Parsons SA and Judd SJ 2020. Influence of granular activated carbon media properties on natural organic matter and disinfection by-product precursor removal from drinking water. Water Research 174, 115613. [PubMed: 32092546]

Gomes HT, Machado BF, Ribeiro A, Moreira I, Rosario M, Silva AM, Figueiredo JL and Faria JL 2008. Catalytic properties of carbon materials for wet oxidation of aniline. J Hazard Mater 159(2–3), 420–426. [PubMed: 18394796]

Han J and Zhang X 2018. Evaluating the Comparative Toxicity of DBP Mixtures from Different Disinfection Scenarios: A New Approach by Combining Freeze-Drying or Rotoevaporation with a Marine Polychaete Bioassay. Environmental Science & Technology 52(18), 10552–10561. [PubMed: 30125089]

Heller-Grossman L, Manka J, Limoni-Relis B and Rebhun M 1993. Formation and distribution of haloacetic acids, THM and tox in chlorination of bromide-rich lake water. Water Research 27(8), 1323–1331.

Hozalski RM, Zhang L and Arnold WA 2001. Reduction of haloacetic acids by Fe0: Implications for treatment and fate. Environmental Science & Technology 35(11), 2258–2263. [PubMed: 11414027]

Jiang J, Han J and Zhang X 2020. Nonhalogenated aromatic DBPs in drinking water chlorination: A gap between NOM and halogenated aromatic DBPs. Environmental Science & Technology 54(3), 1646–1656. [PubMed: 31909989]

Jiang J, Li W, Zhang X, Liu J and Zhu X 2018. A new approach to controlling halogenated DBPs by GAC adsorption of aromatic intermediates from chlorine disinfection: Effects of bromide and contact time. Separation and Purification Technology 203, 260–267.

Jiang J and Zhang X 2018. A smart strategy for controlling disinfection byproducts by reversing the sequence of activated carbon adsorption and chlorine disinfection. Science Bulletin 63, 1167–1169.

Jiang J, Zhang X, Zhu X and Li Y 2017. Removal of intermediate aromatic halogenated DBPs by activated carbon adsorption: A new approach to controlling halogenated DBPs in chlorinated drinking water. Environmental Science & Technology 51(6), 3435–3444. [PubMed: 28199792]

Jiang J-X, Su F, Trewin A, Wood CD, Niu H, Jones JTA, Khimyak YZ and Cooper AI 2008. Synthetic control of the pore dimension and surface area in conjugated microporous polymer and copolymer networks. Journal of the American Chemical Society 130(24), 7710–7720. [PubMed: 18500800]

Johnson RL and Schmidt-Rohr K 2014. Quantitative solid-state 13C NMR with signal enhancement by multiple cross polarization. J Magn Reson 239, 44–49. [PubMed: 24374751]

Levesque S, Rodriguez MJ, Serodes J, Beaulieu C and Proulx F 2006. Effects of indoor drinking water handling on trihalomethanes and haloacetic acids. Water Research 40(15), 2921–2930. [PubMed: 16889815]

Li C, Li L, Sun L, Pei Z, Xie J and Zhang S 2015. Transformation of hydroquinone to benzoquinone mediated by reduced graphene oxide in aqueous solution. Carbon 89, 74–81.

Li Y, Jiang J, Li W, Zhu X, Zhang X and Jiang F 2020. Volatile DBPs contributed marginally to the developmental toxicity of drinking water DBP mixtures against Platynereis dumerilii. Chemosphere 252, 126611. [PubMed: 32443275]

Li Z, Mao J, Chu W and Xu W 2019. Probing the surface reactivity of pyrogenic carbonaceous material (PCM) through synthesis of PCM-like conjugated microporous polymers. Environmental Science & Technology 53(13), 7673–7682. [PubMed: 31244066]

Lifongo L, Bowden D and Brimblecombe P 2010. Thermal degradation of haloacetic acids in water. International Journal of Physical Sciences 5(6), 738–747.

Luo X and Jean-Charles R 2006 Research on oxidation properties of graphite used in HTR-10, Tsinghua Univ., Beijing (China). Inst. of Nuclear and New Energy Technology.

Mao JD and Schmidt-Rohr K 2003. Recoupled long-range C–H dipolar dephasing in solid-state NMR, and its use for spectral selection of fused aromatic rings. Journal of Magnetic Resonance 162(1), 217–227. [PubMed: 12762998]

Marenich AV, Cramer CJ and Truhlar DG 2009. Universal Solvation Model Based on Solute Electron Density and on a Continuum Model of the Solvent Defined by the Bulk Dielectric Constant and Atomic Surface Tensions. Journal of Physical Chemistry B 113(18), 6378–6396. [PubMed: 19366259]

McRae BM, LaPara TM and Hozalski RM 2004. Biodegradation of haloacetic acids by bacterial enrichment cultures. Chemosphere 55(6), 915–925. [PubMed: 15041296]

Ni J, Pignatello JJ and Xing B 2011. Adsorption of aromatic carboxylate ions to black carbon (biochar) is accompanied by proton exchange with water. Environmental Science & Technology 45(21), 9240–9248. [PubMed: 21999243]

Padhye L, Wang P, Karanfil T and Huang C-H 2010. Unexpected role of activated carbon in promoting transformation of secondary amines to N-nitrosamines. Environmental Science & Technology 44(11), 4161–4168. [PubMed: 20446739]

Padhye LP, Hertzberg B, Yushin G and Huang CH 2011. N-nitrosamines formation from secondary amines by nitrogen fixation on the surface of activated carbon. Environ Sci Technol 45(19), 8368–8376. [PubMed: 21863897]

Pals JA, Ang JK, Wagner ED and Plewa MJ 2011. Biological mechanism for the toxicity of haloacetic acid drinking water disinfection byproducts. Environmental Science & Technology 45(13), 5791–5797. [PubMed: 21671678]

Pan Y, Zhang X, Wagner ED, Osiol J and Plewa MJ 2014. Boiling of simulated tap water: Effect on polar brominated disinfection byproducts, halogen speciation, and cytotoxicity. Environmental Science & Technology 48(1), 149–156. [PubMed: 24308807]

Parvez S, Ashby LJ, Kimura YS and Richardson DS 2019. Exposure characterization of haloacetic acids in humans for exposure and risk assessment applications: An exploratory study. International Journal of Environmental Research and Public Health 16(3).

Pei Z, Li C, Xie J, Li L, Sun L, Wen B and Zhang S 2018. Substituent effects on the oxidation reactions of 4-nitrophenol, phenol, 4-methylpheol, and 4-methoxyphenol mediated by reduced graphene oxide in water. Colloids and Surfaces A: Physicochemical and Engineering Aspects 553, 35–41.

Pignatello JJ, Mitch WA and Xu W 2017. Activity and reactivity of pyrogenic carbonaceous matter toward organic compounds. Environmental Science & Technology 51(16), 8893–8908. [PubMed: 28753285]

Plewa MJ, Simmons JE, Richardson SD and Wagner ED 2010. Mammalian cell cytotoxicity and genotoxicity of the haloacetic acids, a major class of drinking water disinfection by-products. Environmental and Molecular Mutagenesis 51(8- 9), 871–878. [PubMed: 20839218]

Plewa MJ and Wagner ED (2015) Recent Advances in Disinfection By-Products, pp. 3–23, American Chemical Society.

Punyapalakul P, Soonglerdsongpha S, Kanlayaprasit C, Ngamcharussrivichai C and Khaodhiar S 2009. Effects of crystalline structures and surface functional groups on the adsorption of haloacetic acids by inorganic materials. Journal of Hazardous Materials 171(1), 491–499. [PubMed: 19592162]

Richardson SD 2002. The role of GC-MS and LC-MS in the discovery of drinking water disinfection by-products. Journal of Environmental Monitoring 4(1), 1–9. [PubMed: 11871687]

Rodriguez MJ, Serodes JB and Levallois P 2004. Behavior of trihalomethanes and haloacetic acids in a drinking water distribution system. Water Res 38(20), 4367–4382. [PubMed: 15556212]

Serjeant EP and Dempsey B (1979) IUPAC chemical data series: Ionisation constants of organic acids in aqueous solution, Pergamon Press, Oxford.

Summers RS, Benz MA, Shukairy HM and Cummings L 1993. Effect of separation processes on the formation of brominated THMs. Journal AWWA 85(1), 88–95.

Tang XP, Kleinhammes A, Shimoda H, Fleming L, Bennoune KY, Sinha S, Bower C, Zhou O and Wu Y 2000. Electronic structures of single-walled carbon nanotubes determined by NMR. Science 288(5465), 492. [PubMed: 10775103]

Tinker SC, Moe CL, Klein M, Flanders WD, Uber J, Amirtharajah A, Singer P and Tolbert PE 2009. Drinking water residence time in distribution networks and emergency department visits for gastrointestinal illness in Metro Atlanta, Georgia. Journal of water and health 7(2), 332–343. [PubMed: 19240359]

Tung H. h. and Xie YF 2009. Association between haloacetic acid degradation and heterotrophic bacteria in water distribution systems. Water Research 43(4), 971–978. [PubMed: 19070347]

Tung H. h. and Xie YF 2011. Evaluate HAA removal in biologically active carbon filters using the ICR database. Frontiers of Environmental Science & Engineering in China 5(4), 489–496.

Tung HH, Unz RF and Xie YF 2006. HAA removal by GAC adsorption. Journal - American Water Works Association 98(6), 107–112.

USEPA 1995 Methods for the determination of organic compounds in drinking water: supplement 3. USEPA (ed).

USEPA 2000 Wastewater Technology Fact Sheet. Agency, E.P. (ed), U.S. EPA, Washington, D.C.

USEPA (2003) Method 552.3: Determination of haloacetic acids and dalapon in drinking water by liquid-liquid microextraction, derivatization, and gas chromatography with electron capture detection, Revision 1.0, U.S. EPA, Washington, D.C.

USEPA 2016 Six-year review 3 technical support document for disinfectants/disinfection byproducts rule, United States Environmental Protection Agency.

van der Zee FP, Bisschops IAE, Lettinga G and Field JA 2003. Activated carbon as an electron acceptor and redox mediator during the anaerobic biotransformation of azo dyes. Environmental Science & Technology 37(2), 402–408. [PubMed: 12564915]

Villanueva CM, Kogevinas M and Grimalt JO 2003. Haloacetic acids and trihalomethanes in finished drinking waters from heterogeneous sources. Water Res 37(4), 953–958. [PubMed: 12531279]

Wagner ED and Plewa MJ 2017. CHO cell cytotoxicity and genotoxicity analyses of disinfection by-products: An updated review. Journal of Environmental Sciences 58, 64–76.

WQA 2016 Granular activated carbon (GAC) fact sheet, Water Quality Association, National Headquarters and Laboratory, LIsle, Illinois.

Xie J, Li L, Sun L, Pei Z, Wen B and Xing B 2017. Reduced graphene oxide-catalyzed oxidative coupling reaction of 4-methoxyphenol in aerobic aqueous solution. Carbon 121, 418–425.

Xie YF (2003) Disinfection byproducts in drinking water: Formation, analysis, and control, CRC Press.

Xu W, Dana KE and Mitch WA 2010. Black carbon-mediated destruction of nitroglycerin and RDX by hydrogen sulfide. Environmental Science & Technology 44(16), 6409–6415. [PubMed: 20704242]

Xu W, Pignatello JJ and Mitch WA 2013. Role of black carbon electrical conductivity in mediating hexahydro-1,3,5-trinitro-1,3,5-triazine (RDX) transformation on carbon surfaces by sulfides. Environ Sci Technol 47(13), 7129–7136. [PubMed: 23725551]

Xu W, Segall ML and Li Z 2020a. Reactivity of pyrogenic carbonaceous matter (PCM) in mediating environmental reactions: Current knowledge and future trends. Frontiers of Environmental Science & Engineering 14(5).

Xu W, Walpen N, Keiluweit M, Kleber M and Sander M 2021. Redox properties of pyrogenic dissolved organic matter (pyDOM) from biomass-derived chars. Environ Sci Technol.

Xu X, Gujarati PD, Okwor N, Sivey JD, Reber KP and Xu W 2022. Reactivity of chloroacetamides toward sulfide + black carbon: Insights from structural analogues and dynamic NMR spectroscopy. Science of The Total Environment 803, 150064. [PubMed: 34525700]

Xu X, Sivey JD and Xu W 2020b. Black carbon-enhanced transformation of dichloroacetamide safeners: Role of reduced sulfur species. Sci Total Environ 738, 139908. [PubMed: 32531604]

Zhang S. h., Miao D. y., Tan L, Liu A. l. and Lu W. q. 2015. Comparative cytotoxic and genotoxic potential of 13 drinking water disinfection by-products using a microplate-based cytotoxicity assay and a developed SOS/umu assay. Mutagenesis 31(1), 35–41. [PubMed: 26188195]

Zhang X and Minear RA 2002. Decomposition of trihaloacetic acids and formation of the corresponding trihalomethanes in drinking water. Water Research 36(0043–1354 (Print)).

Zhao HQ, Huang SQ, Xu WQ, Wang YR, Wang YX, He CS and Mu Y 2019. Undiscovered mechanism for pyrogenic carbonaceous matter-mediated abiotic transformation of azo dyes by sulfide. Environ Sci Technol 53(8), 4397–4405. [PubMed: 30908036]

Zhao Y and Truhlar DG 2008. How Well Can New-Generation Density Functionals Describe the Energetics of Bond-Dissociation Reactions Producing Radicals? The Journal of Physical Chemistry A 112(6), 1095–1099. [PubMed: 18211046]

Zhou H and Xie YF 2002. Using BAC for HAA removal: Part 1: Batch Study. Journal - AWWA 94(4), 194–200.

Highlights

- Complete abiotic transformation of Br3AA in 30 min with powder activated carbon.
- Rapid haloacetic acid conversion to volatile trihalomethanes by pyrogenic carbon.
- Pyrogenic carbon lowered the activation energy for haloacetic acid decarboxylation.
- A combined experimental and computational approach was employed.
- COOH catalyzed HAA C-C bond breaking and facilitated H+ transfer to form THMs.

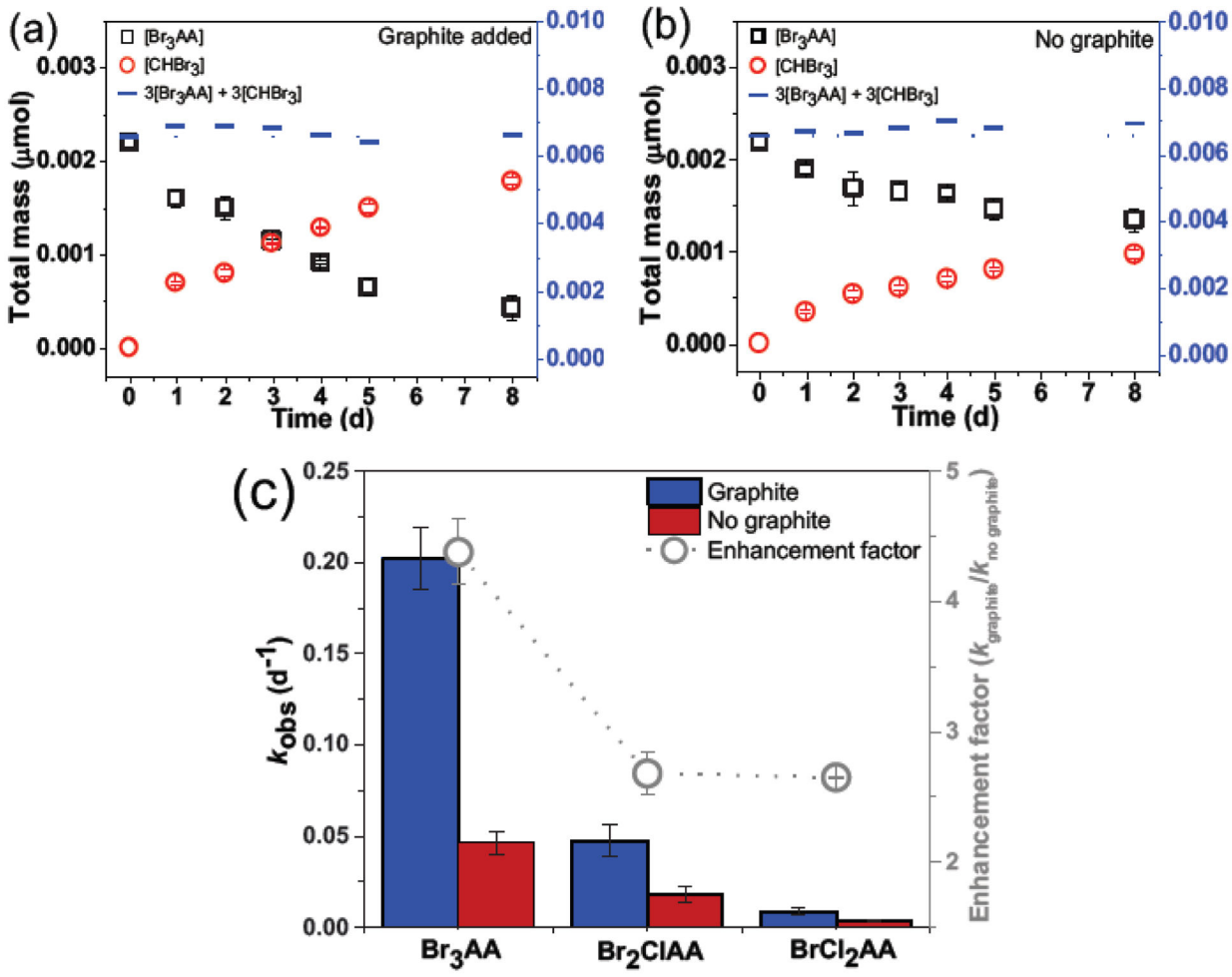

Fig. 1.

Tribromoacetic acid (Br_3AA; □) degradation and bromoform ($CHBr_3$; ○) formation over time. Mass balance (—) on bromine is calculated as (a,b) $3[Br_3AA]+3[CHBr_3]$. Reaction conditions: $[Br_3AA]_0$=50 μg·L^{-1}; solid-to-liquid ratio: 23.08 g·L^{-1} in 10 mM KH_2PO_4/K_2HPO_4 (pH 7.0±0.1); 25°C in darkness, 30 rpm; controls were without graphite. Error bar represents standard deviation of experimental duplicates. (c) Pseudo first-order degradation rate constants and enhancement factors for Br_3AA ($R^2_{graphite}$=0.97; $R^2_{no\ graphite}$=0.91), Br_2ClAA ($R^2_{graphite}$=0.85; $R^2_{no\ graphite}$=0.86), and $BrCl_2AA$ ($R^2_{graphite}$=0.92; $R^2_{no\ graphite}$=0.90) with/without graphite.

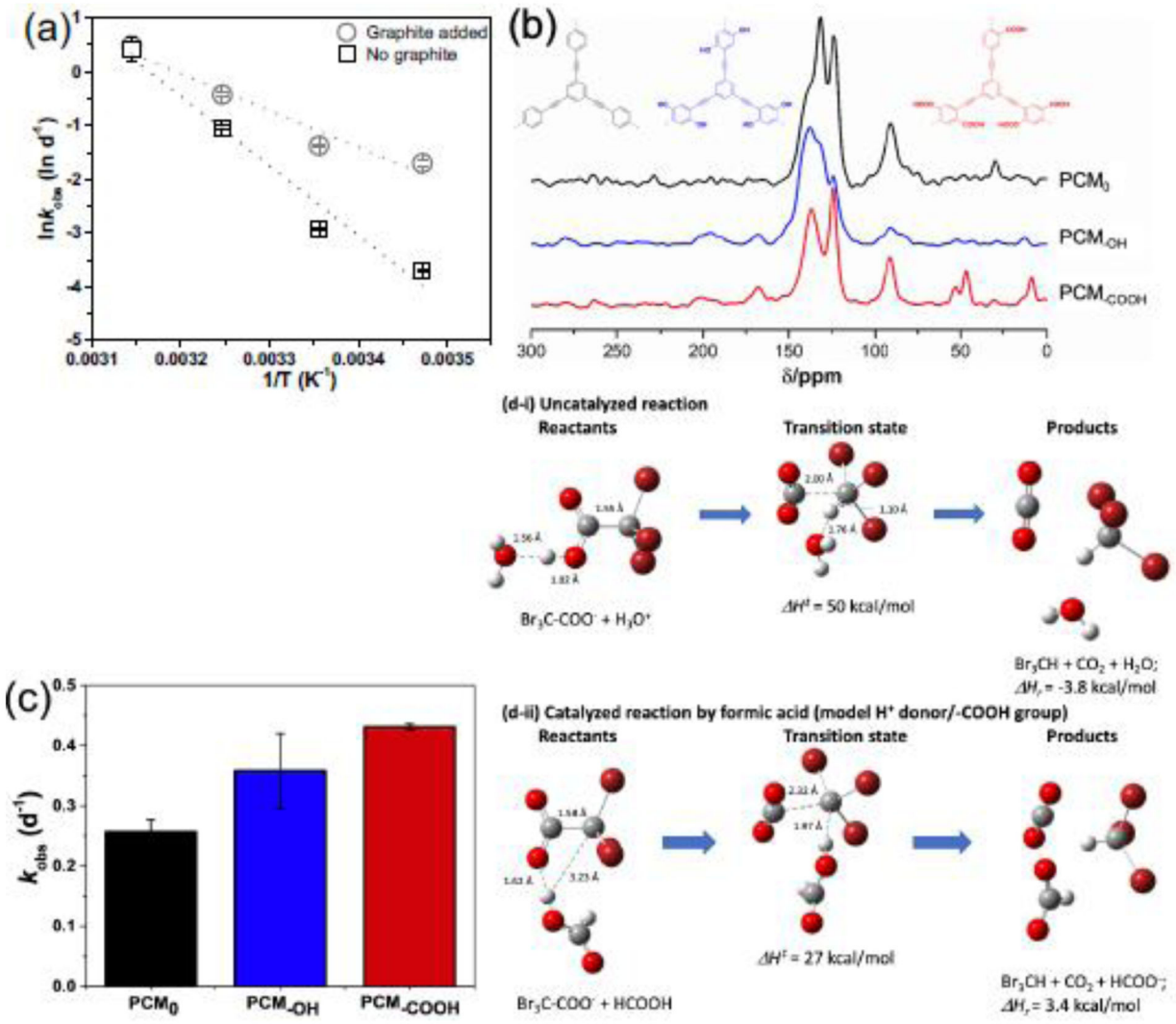

Fig. 2.

(a) Arrhenius plot $k_{obs} = Ae^{-E_a/RT}$ for Br_3AA degradation without (□) and with (○) graphite over time at 15°C, 25°C, 35°C, and 45°C in darkness. The calculated Br_3AA decay activation energies (E_a) were 13.6±2.2 and 25.7±3.2 kcal·mol^{-1} with/without graphite. (b) Solid state ^{13}C multiCP/MAS NMR spectra of PCM_0 (Li et al., 2019), PCM_{-OH} (Li et al., 2019), and PCM_{-COOH}. All the spectra were recorded at a spinning speed of 14 kHz with a 90° ^{13}C pulse-length of 4 μs. (c) Pseudo first-order Br_3AA degradation rate constants with PCM_0, PCM_{-OH}, and PCM_{-COOH}. (d) Optimized structures for reactants, transition state, and products of (i) Reaction (1) and (ii) Reaction (2) based on DFT simulation.

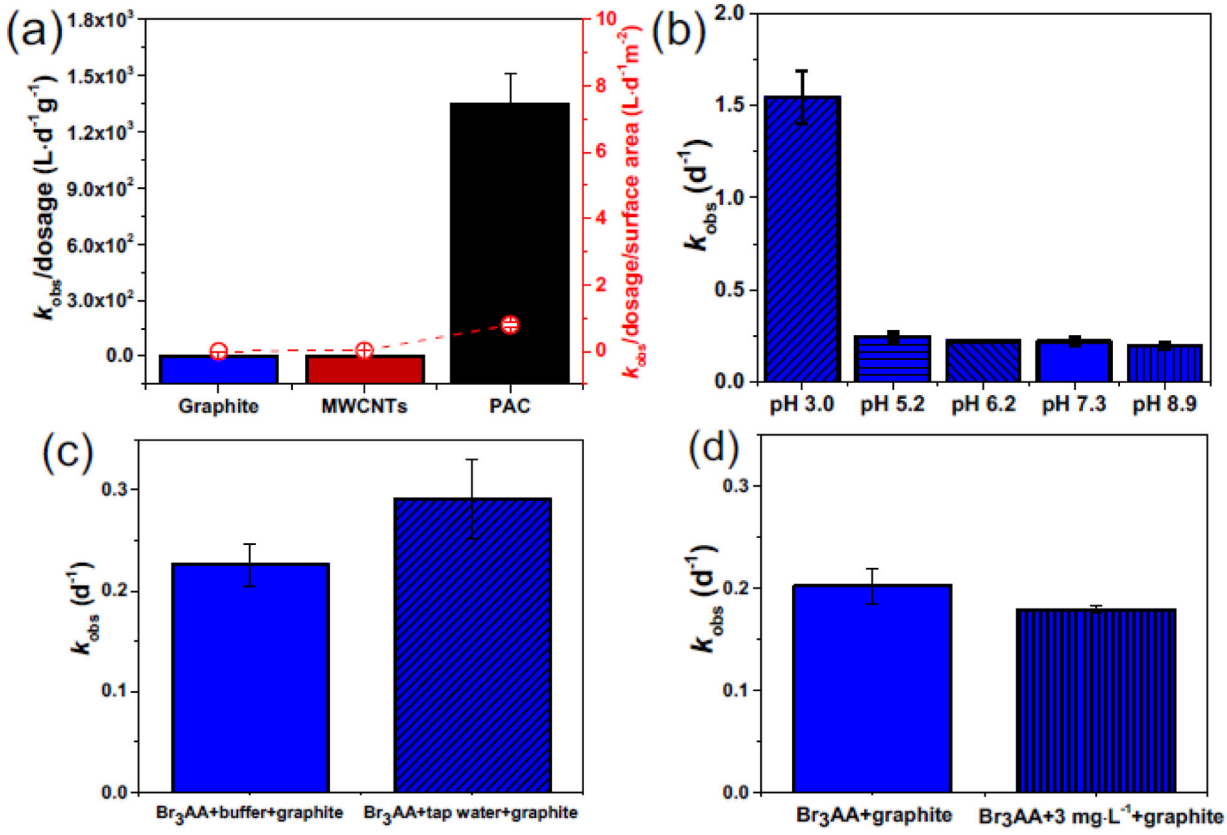

Fig. 3.

(a) Pseudo first-order Br_3AA decay kinetics with graphite, MWCNTs, and PAC normalized to PCM dosage (left axis), and surface area (right axis). (b) Br_3AA decay kinetics with graphite at pH 3.0 (k_{obs}=1.49±0.16 d^{-1}; R^2=0.92), 5.2 (k_{obs}=(2.46±0.25)×10^{-1} d^{-1}; R^2=0.96), 6.2 (k_{obs}=(2.30±0.01)×10^{-1} d^{-1}; R^2=0.99), 7.3 (k_{obs}=(2.22±0.18)×10^{-1} d^{-1}; R^2=0.97), and 8.9 (k_{obs}=(1.97±0.18)×10^{-1} d^{-1}; R^2=0.96). (c) Br_3AA decay kinetics with 10 mM KH_2PO_4/K_2HPO_4 (k_{obs}=(2.26±0.21)×10^{-1} d^{-1}; R^2=0.97) and tap water (k_{obs}=(2.91±0.06)×10^{-1} d^{-1}; R^2=0.99). (d) Br_3AA decay kinetics in the presence of graphite with (k_{obs}=(1.79±0.04)×10^{-1} d^{-1}; R^2=0.99) or without (k_{obs}=(2.02±0.17)×10^{-1} d^{-1}; R^2=0.97) 3 mg·L^{-1} Suwannee River NOM. Reaction conditions: $[Br_3AA]_0$=50 μg·L^{-1}; solid-to-liquid ratio: 0.77 or 23.08 g·L^{-1}; 25°C in darkness, 30 rpm; controls were without powder. Error bar represents standard deviation of experimental duplicates.

Table 1.

Calculated adsorption, desorption, and surface transformation reaction rate constants of Br_3AA with graphite, PCM_0, PCM_{-OH}, or PCM_{-COOH} at 25°C. Details on Langmuir kinetic model fitting and adsorption kinetics are in Text S4, Fig. S5, and Fig. S8.

Powder	k_a ($L \cdot \mu g^{-1} \cdot d^{-1}$)	k_d (d^{-1})	k_{rxn} (d^{-1})
Graphite	$(4.55\pm0.35)\times10^{-2}$	$(4.67\pm0.39)\times10^{1}$	$(3.52\pm0.92)\times10^{2}$
PCM_0	$(1.60\pm0.32)\times10^{-1}$	$(1.86\pm0.36)\times10^{2}$	$(2.68\pm0.01)\times10^{2}$
PCM_{-OH}	$(9.29\pm0.68)\times10^{-2}$	$(1.33\pm0.22)\times10^{2}$	$(1.97\pm0.03)\times10^{3}$
PCM_{-COOH}	$(6.56\pm0.13)\times10^{-2}$	$(1.18\pm0.16)\times10^{2}$	$(4.34\pm0.01)\times10^{3}$